

Lawrence Berkeley National Laboratory

Recent Work

Title

MULTIWIRE PROPORTIONAL CHAMBERS FOR BIOMEDICAL APPLICATION

Permalink

<https://escholarship.org/uc/item/77z0x8f3>

Author

Kaplan, S.N.

Publication Date

1972-06-01

MULTIWIRE PROPORTIONAL CHAMBERS FOR
BIOMEDICAL APPLICATION

S. N. Kaplan, L. Kaufman, V. Perez-Mendez,
K. Valentine

June 1972

AEC Contract No. W-7405-eng-48



For Reference

Not to be taken from this room

DISCLAIMER

This document was prepared as an account of work sponsored by the United States Government. While this document is believed to contain correct information, neither the United States Government nor any agency thereof, nor the Regents of the University of California, nor any of their employees, makes any warranty, express or implied, or assumes any legal responsibility for the accuracy, completeness, or usefulness of any information, apparatus, product, or process disclosed, or represents that its use would not infringe privately owned rights. Reference herein to any specific commercial product, process, or service by its trade name, trademark, manufacturer, or otherwise, does not necessarily constitute or imply its endorsement, recommendation, or favoring by the United States Government or any agency thereof, or the Regents of the University of California. The views and opinions of authors expressed herein do not necessarily state or reflect those of the United States Government or any agency thereof or the Regents of the University of California.

MULTIWIRE PROPORTIONAL CHAMBERS FOR BIOMEDICAL APPLICATION

S. N. KAPLAN,* L. KAUFMAN,† V. PEREZ-MENDEZ,† K. VALENTINE*

Lawrence Berkeley Laboratory

University of California

Berkeley, California

June 1972

ABSTRACT

Multiwire proportional chambers with delay-line readouts, currently used for particle trajectory measurements in high-energy physics, are being adapted for a variety of biomedical applications including x radiography, neutron radiography, and radioisotope imaging. This paper describes chamber-design features and gives calculated and measured efficiency and resolution data. Sample radiographic images taken with prototype chambers are shown.

* Also, Department of Nuclear Engineering, University of California, Berkeley.

† Also, Department of Radiology, University of California, San Francisco.

1. Introduction

Multiwire proportional chambers (MWPC) with the ability to detect ionizing radiations as well as to record the position where the ionizing particles strike the chamber are a modern development based upon the properties of the old proportional counters¹).

In physics applications, these chambers are used for detecting the trajectories of charged particles to accuracies of a fraction of a millimetre²). In the applications we discuss here, where fluxes of gamma rays and neutrons are of interest, detection is accomplished by virtue of the secondary charged particles produced either in the gas of the chamber or in solid converters which enclose the gas volume of the chambers. Where the interactions take place in the gas, as in the case of x-ray and low-energy gamma-ray detection, we also make use of the proportional feature of these chambers in order to discriminate against unwanted radiations. For such purposes we use gas mixtures such as xenon or argon with a quenching gas,³) but exclude any of the electronegative gases which enhance the multiplication and produce larger signals at the cost of energy resolution⁴).

In the following sections we discuss the basic construction of the chambers that have been used and are proposed for use in biomedical applications. The digitizing method in all of these cases employs electromagnetic-delay-line readout⁵). The medical applications we discuss cover the use of these chambers for conventional x-ray and neutron imaging as well as isotope camera applications in nuclear medicine, where various-energy gamma-ray-emitting isotope distributions

in body organs are studied. Other **possible biophysics** applications include diffraction-pattern imaging in x-ray crystallographic studies of complex organic crystals, where the intensity distributions are difficult to measure by conventional means, and radioisotope chromatography.

2. Basic-Chamber Construction, Digitized Readout, and Display

In all of these applications we use a similar chamber construction. This basic chamber is shown schematically in fig. 1. It consists of three grids of parallel wires enclosed in a gas-tight envelope. The spacing between grids varies from 3 - 10 millimetres, and that between wires varies from 1 - 3 millimetres, depending on the size of the chamber and the spatial resolution required. The center grid, on which the avalanche multiplication occurs, consists of gold-plated tungsten wires typically 15 - 25 microns in diameter; this grid is held at a high positive potential relative to the two outside ones, which are usually held at ground potential. The wires of the central grid are connected to a common bus bar and pulse-height information can be obtained from it.

The two outer grids which are used to obtain the spatial information consist of larger diameter wires, typically 50 microns or larger. In order to provide a rectilinear system of coordinates these two grids have their wire axes mutually orthogonal.

The coordinates of an ionizing event are determined by the use of electromagnetic delay lines capacitatively coupled to each of the orthogonal planes of ground-grid wires. In these grids we make use

of the prompt, positive signals induced on them by the avalanche process after the electrons have been collected on the central grid wires²). In order to enable the induced signals on the ground plane wires to produce a voltage signal of the right shape, these ground grid wires are decoupled from each other and ground through 200 k Ω isolating resistors. The construction and characteristics of the delay lines have been described in detail elsewhere⁵). Fig. 2 shows the construction of a delay line and the pulse-shape characteristics of a signal coupling into and out of the line.

A signal that indicates the occurrence of an ionizing event is obtained from the central plane through an RC network with a time constant of 500 nsec. This signal is processed by the technique of differentiation and zero-crossing, and is used to start two time-to-height converters. Similarly processed signals obtained from each delay line are used to stop the converters, one from the x-coordinate line and one from the y-coordinate line.

Analog image reconstruction and display is done by using the outputs from the time-to-height converters to drive the x-y deflection plates of a CRT, while simultaneously a z unblank signal is applied, as shown in fig. 3a. The resultant pattern of dots may then be photographed with a Polaroid camera. Both Tektronix 536 and 602 oscilloscopes have been used for this type of image display. Rates up to 10^5 events/sec have been recorded when a pile-up rejector circuit was used to eliminate multiple events occurring within the delay lines' delay interval and the dead time of the electronics. This rate is

presently limited by the recording electronics. The chambers and the delay lines themselves have a dead time of less than 1 μ sec.

An alternative method of recording the images (shown schematically in fig. 3b) is to digitize the time-delay signals from the chamber by use of a clock and 200 MHz scalars, and then store the coordinates of each event on magnetic tape, disc, or random-access core.

3. Special Chambers for Biomedical Applications

(a) X-radiography

For the detection and imaging of x-rays, xenon is used as the principal constituent of the proportional gas. Used in this manner, these chambers offer the capability of recording large-area images with very high efficiency. Although the ultimate resolution of these chambers is inferior to that of film, the comparison of picture quality is not too unfavorable, since factors other than film resolution frequently limit the performance of more conventional x-ray systems (i.e., focal-spot size, geometry, small-angle scattering, subject movement, etc.). Since the chambers operate in the proportional mode, they also yield the energy of the detected photon with spectral discrimination on the order of 15% FWHM. Thus, they can be used for the imaging of characteristic radiation, or to select a narrow band of x-ray energies from the wide-range output of a standard tube. This permits optimization of energy, and therefore contrast, for the study of interest. Fig. 4 shows energy spectra obtained with various sources.

X-ray imaging studies were performed⁶) with a 20×20 cm² chamber, with the multiplication plane made of 20 μ m wires with a pitch of

16 wires/inch, at 45° to the outside planes. By using the volume between these outside planes and the windows as drift regions, we achieved a total xenon mass of 2.21×10^{-2} g/cm².

The chamber efficiency and sensitivity (in events per cm² for 1 roentgen) were calculated and are shown in fig. 5. Measurements to corroborate these calculations were performed at 22 keV and 60 keV.

We determined the modulation transfer function (MTF) of the chamber along the x and y directions by recording the data from three resolution-grid patterns consisting of lead slats 4, 2, and 1 mm wide spaced by 4, 2, and 1 mm distances respectively. The object contrast is taken to be 100%, so the value of the MTF is determined from the measured image contrast. For these tests we used a 22 keV ¹⁰⁹Cd source 3 mm in diameter placed 12 cm above the grid pattern, which was located on the face of the chamber. The MTF fitted to the data points and corrected for source size is shown in fig. 6. Figs. 7 and 8 show pictures obtained with this chamber by using 5.9 keV and 22 keV sources respectively. The delivered radiation doses for these pictures are quite small. However, they represent 2 to 5×10^4 events-cm⁻² corresponding, at the present maximum data collection rate of the system ($\sim 10^5$ sec⁻¹), to exposure times on the order of 1/4 - 1/2 sec-cm⁻² of image.

Therefore, the system as now realized would be useful chiefly for specialized applications where either the subject of interest can be immobilized or where resolution is not of paramount importance but dosage is. Prolonged medical fluoroscopy, presently requiring large

radiation doses, is an obvious potential application, particularly if the data collection rate were increased beyond the limit presently imposed only by the imaging electronics.

(b) Neutron radiography

The basic system is modified for neutron imaging by coating the inside surfaces of the chamber windows with material that converts neutrons to charged particles. Thermal and epithermal sensitivity may be achieved with a ^{10}B coating and fast-neutron sensitivity with a polyethelene coating. Because of the chamber's proportional response, the heavy charged particles produced in these converting materials are easily distinguished from gamma and x-ray background.

The response of an argon-filled chamber with a ^{10}B converter to a narrow beam of neutrons is illustrated in fig. 9. The figure shows the loci of track endings, in the chamber, of α particles originating in each of 25 equal-thickness layers of the converter. In a beam of 0.025 eV neutrons, a layer of ^{10}B that is one α -particle-range thick (5 μm) absorbs about 20% of the incident beam and has an intrinsic efficiency of 5% for yielding α particles that reach the chamber gas. The numbers that appear on alternate curves in fig. 9 give the percent of this yield contributed by α particles stopping on the curve. The efficiency and resolution of various B-screen systems may be analyzed by means of this set of curves. For example, reducing the B thickness removes the contribution from the innermost curves, and overcoating the B with non-converting material such as Al removes the contribution from the outermost curves. The effect of energy discrimination is

illustrated by the two circular segments. They are curves of constant energy and correspond to α -energy depositions of 0.1 and 1.0 MeV respectively. Varying the chamber thickness has the effect of flattening longitudinally all curves corresponding to an α range greater than the chamber thickness. Sample analyses of converter screen performance have been described in detail elsewhere⁷).

The performance of a small natural-boron-lined prototype chamber, 3×4 cm sensitive area, has been tested for thermal-neutron imaging. With 2 mm wire spacing and a single neutron-converting surface we have achieved 0.5% detection efficiency and 2 mm 10-90% resolution of a Cd knife edge or a Lucite step.

An example of image quality and information content is shown in fig. 10. This prototype chamber has also been used to obtain quantitative measurements of Lucite-step thicknesses. As with any electronic counter the precision of such measurements is limited only by counting statistics and background.

The modulation transfer function of the chamber was measured by using periodic arrays of cadmium strips glued to a thin Al backing. An MTF calculated from the data of fig. 11 is compared with the measured points. The predicted sign of the contrast ratio at the 5 cm^{-1} point has been confirmed experimentally.

Extrapolating the measured efficiency of this single-screen natural-boron chamber to one with two optimum-thickness converting surfaces of ^{10}B for slow neutrons and a single surface of CH_2 for fast neutrons (since for n-p scattering only an upstream surface would yield

protons to the chamber gas), we may predict the following efficiency characteristics.

<u>Neutron spectrum</u>	<u>Efficiency (%)</u>	<u>Approximate neutron dose at chamber for a 1 n-mm⁻² image</u>	
		<u>(n - cm⁻²)</u>	<u>(mrem)</u>
Thermal	7	1.4×10^3	1.5×10^{-3}
1 eV	1.2	8.0×10^3	8.0×10^{-3}
Fission	0.1	1.0×10^5	3.4
14 MeV	0.3	3.2×10^4	2.2

A 25 x 25 cm, two-surface, ¹⁰B chamber with 1 mm wire spacing is under construction. The converter-covered chamber windows are easily interchangeable and will permit testing of a fast-neutron converter also.

Although considerable research has been done over the past several years to investigate diagnostic applications for neutron radiography⁸), we are not familiar with any in vivo clinical usage. Recently, however, neutron radiography has been successfully employed to determine the adequacy of bone margins in a surgically removed tumorous jaw bone⁹). A high-efficiency imaging system as described above with the capabilities for digital processing could permit quantitative in vitro diagnostics, as well as extend the range of in vivo experimentation.

(c) Radioisotope imaging

In this application the device is used to image the spatial distribution of an internally administered γ -emitting radioisotope. For this purpose a parallel-hole collimator is used to limit the

photons reaching the MWPC to those which travel in a direction nearly perpendicular to it. Three collimators have been used: a Nuclear-Chicago High Resolution Low Energy collimator with a useful area of $27 \times 27 \text{ cm}^2$ (NC1); a Nuclear-Chicago High Sensitivity Low Energy collimator with the same area (NC2); and a low-energy collimator assembled from 2.54 cm lengths of 0.0238-cm o.d., 0.015-cm wall, steel tubing, in a hexagonal close-packed configuration, with an area of $10 \times 12 \text{ cm}^2$ (STC). These collimators have a resolution of approximately 2 mm at the surface.

The MWPC used here¹⁰) had an active area of $30.5 \times 30.5 \text{ cm}^2$, a center wire grid with a pitch of 12 wires per inch, and was xenon filled with an effective mass of $2.21 \times 10^{-2} \text{ gm-cm}^{-2}$ of xenon. Its efficiency was the same as that shown in fig. 5.

Fig. 12 shows transmission images of various bar patterns obtained with 22 keV and 60 keV photons. As the energy increases, the resolution, which approaches 1 mm at 22 keV, degrades to about 2 mm at 60 keV. This degradation is due to the range of the photoelectrons and can be reduced or eliminated by operating the chamber at higher-than-atmospheric pressure. The figure also shows the effect of Lucite absorbers--interposed between the chamber and the bar pattern--on the imaging properties of 60 keV photons. In fig. 13 we show a comparison between images obtained with MWPC and a conventional scintillation camera¹¹).

The xenon-filled MWPC affords a very efficient low-cost method for imaging the distributions of internally administered radioisotopes that emit photons in the energy region below 100 keV. Radioisotopes used in

nuclear medicine that can be imaged with this system are ^{125}I , ^{197}Hg , ^{195}Au , ^{133}Xe , and, as availability increases, ^{123}I . The most commonly used radioisotope, ^{99}Tc , can be imaged but with lower efficiency and poorer resolution than with a scintillation camera.

(d) External excitation laminographic imaging

This is a modification of ordinary radioisotope imaging; it will permit laminographic display of the thyroid without administration of radiopharmaceuticals to the patient. An external, collimated, line source of x- or γ -rays is used to excite the K x-ray lines of natural iodine in a patient's thyroid in such a way that excitation is limited to well-defined planes parallel to the plane of the imaging chamber (fig. 14).

The present irradiation-system design¹²⁾ employs a symmetrical arrangement of two line sources of ^{241}Am (fig. 15). Its general availability and long lifetime--together with the uniformity of irradiation from its 60 keV γ -ray in this symmetric arrangement--make ^{241}Am an ideal choice for the excitation source. The detector is a xenon-filled chamber of area $11 \times 13 \text{ cm}^2$. Its detection efficiency is 18% for the 28.6 keV $\text{K}\alpha$ x-ray from iodine.

Normally-incident x-rays are selected with a high-resolution parallel-hole collimator. The collimator has an area of $10 \times 12 \text{ cm}^2$ and allows for a geometric resolution of 0.3 and 0.5 cm for objects on the collimator surface and 2.5 cm away respectively.

Radiation exposures (limited to the excited area) will be on the order of 1 rad/min, with a sensitivity of about $700 \text{ counts-cm}^{-3}\text{-rad}^{-1}$.

These rates will make possible the acquisition of high-quality laminographs in a few minutes.

(e) Positron imaging

The lead collimator necessary for single-gamma-ray imaging systems is by far the most inefficient, expensive, and cumbersome element in the system. The ensuing resolution--as discussed above--of the whole system is in general limited by the collimator characteristics.

In order to avoid the use of collimators, radioisotope scanning and imaging have been done by using a positron emitter as the labelling radioactive element¹³). The subsequent annihilation of the positron into two back-to-back 0.511 MeV γ -rays can provide the spatial-distribution information on the tracer material if these γ -rays are detected in coincidence in two separate detectors placed on either side of the source distribution. This allows one to determine a line on which the emitter is located; by accumulation of a statistically meaningful number of these lines, the positron source distribution can be mapped.

Large-area devices--such as wire chambers--are well suited to this application, in spite of their low (1-2%) detection efficiency for 0.51 MeV γ -rays. Some initial work on a positron camera using wire spark chambers has been done¹⁴), and we plan to continue this work by using the MWPC.

In this work we propose to use two MWPC's of dimensions 50 x 50 cm. The γ conversion is done on two corrugated lead-plate converters which will give a total detection efficiency of 1% for each chamber. For the

coincidence-resolving time of the chambers (50 nsec) and allowing a maximum of 10% accidental coincidences, we estimate that we can use source strengths on the order of 1 millicurie, which will give approximately 5000 counts/sec when the chambers are spaced at 50 cm.

Although such a source strength is quite high for general medical imaging, it is suitable for use with $^{11}_{6}\text{C}$ (β^+ , $T_{1/2} = 20.5$ min) and $^{15}_{8}\text{O}$ (β^+ , $T_{1/2} = 2.1$ min), which are biologically very interesting elements and do not have any other suitable isotopes for imaging purposes.

(f) X-ray crystallography detectors

Another application of MWPC's on which we are working is the use of a chamber of this type as a detector for x-ray crystallography. In organic crystals of a complicated nature, the intensities of the diffraction spots are mapped out carefully by using a number of modifications of the crystal in order to unravel the crystal structure. Since these crystals are often very fragile and deteriorate rapidly while exposed to the primary x-ray beam (usually the 8 keV K_{α} line of copper), it is obvious that a device that can map in parallel the intensity of a large number of the diffraction spots will present many advantages over the standard moving-detector arrangements.

4. Conclusions

Prototype demonstrations have been made of radiographic imaging capabilities of multiwire proportional chambers with delay-line readouts. For low-energy radioisotope imaging they offer a sensitive, high-resolution, low-cost alternative to the γ -ray camera. They can produce

moderate resolution x-radiographs at extremely low incident dosages and, in conjunction with a conversion screen, may be adapted for similar resolution, high-efficiency, neutron radiographic imaging.

Presently the main limitations on spatial resolution are due to wire spacing and track length. This resolution should be improvable by reducing wire spacing and by reducing effective track length. The latter may be accomplished by reducing grid spacing (i.e., the thickness of the sensitive region) and/or by pressurizing the chambers. In the Xe-filled chamber, efficiency would increase also in direct proportion to pressurization. Inasmuch as the time resolution of the chamber and delay line system is on the order of 1 μ sec, an order-of-magnitude improvement of the present data handling rate ($\sim 10^5$ /sec) should be readily achievable.

Acknowledgements

We would like to thank many members of the staff at Lawrence Berkeley Laboratory and at University of California Medical School and the Berkeley Research Reactor for their help and cooperation in projects discussed above. Specifically, we acknowledge the very great help given to us by Dr. John Sperinde, Ronald Grove, Gerald Stoker, and Ray Fuzesy (LBL) and Drs. Malcolm Powell and David Price (UCSF).

References

1. G. Charpak, Ann. Rev. Nucl. Sci. 20 (1970) 221.
This review paper has an extensive bibliography and covers most of the work up to 1970.
2. R. Grove, K. Lee, V. Perez-Mendez and J. Sperinde, Nucl. Instr. and Meth. 89 (1970) 257.
3. R. Z. Fuzesy, J. Jaros, L. Kaufman, J. Marriner, S. Parker, V. Perez-Mendez and S. Redner, Nucl. Instr. and Meth. 100 (1972) 267.
4. R. Bouclier, G. Charpak, Z. Dimcovski, G. Fischer, F. Sauli, G. Coignet and G. Flugge, Nucl. Instr. and Meth. 88 (1970) 149.
5. A. Rindi, V. Perez-Mendez and R. Wallace, Nucl. Instr. and Meth. 77 (1970) 325; and R. Grove, I. Ko, B. Leskovar and V. Perez-Mendez, Nucl. Instr. and Meth. 99 (1972) 381.
6. L. Kaufman, V. Perez-Mendez, J. Sperinde and G. Stoker, Am. J. Roentgenol., Radium Therapy Nucl. Med. 113 (1971) 378.
7. K. Valentine, S. Kaplan, L. Kaufman and V. Perez-Mendez, IEEE Trans. Nucl. Sci. NS-19 (Feb. 1972) 374.
8. See, for example, Roland Buchet, Journal de Radiologie, d'Electronique et de Medicien Nucleaire 51 (1970) 269. Reprinted in English translation in "Neutron Sources and Applications," Proceedings of the ANS National Topical Meeting, April 19-21, 1971, Augusta, Georgia, CONF-710402 II, II-37 (1971) and M. Brown, ibid. I, II-19.

9. W. L. Whittemore and P. J. Boyne, *Research/Development*, July, 1971, p. 22; P. J. Boyne and W. L. Whittemore, *Oral Surgery, Oral Medicine, Oral Pathology* 31 (1971) 152.
10. L. Kaufman, V. Perez-Mendez, D. Shames and G. Stoker, *IEEE Trans. Nucl. Sci.* NS-19, (June 1972) 169.
11. See, for example, Hal O. Anger, in Instrumentation in Nuclear Medicine 1, edited by G. J. Hine (Academic Press, New York, 1967), p. 486.
12. L. Kaufman, V. Perez-Mendez, M. Powell and G. Stoker, *IEEE Trans. Nucl. Sci.* NS-19 (Feb. 1972) 46.
13. See ref. 11 and Saul Aronow, ibid. p. 461.
14. L. Kaufman, V. Perez-Mendez and H. Wollenberg, Lawrence Berkeley Laboratory Report UCID-3184 (1968), unpublished.

Figure Captions

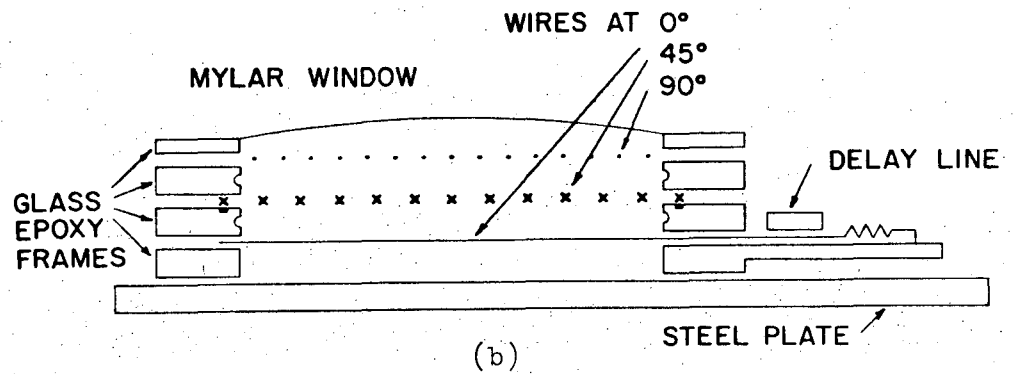
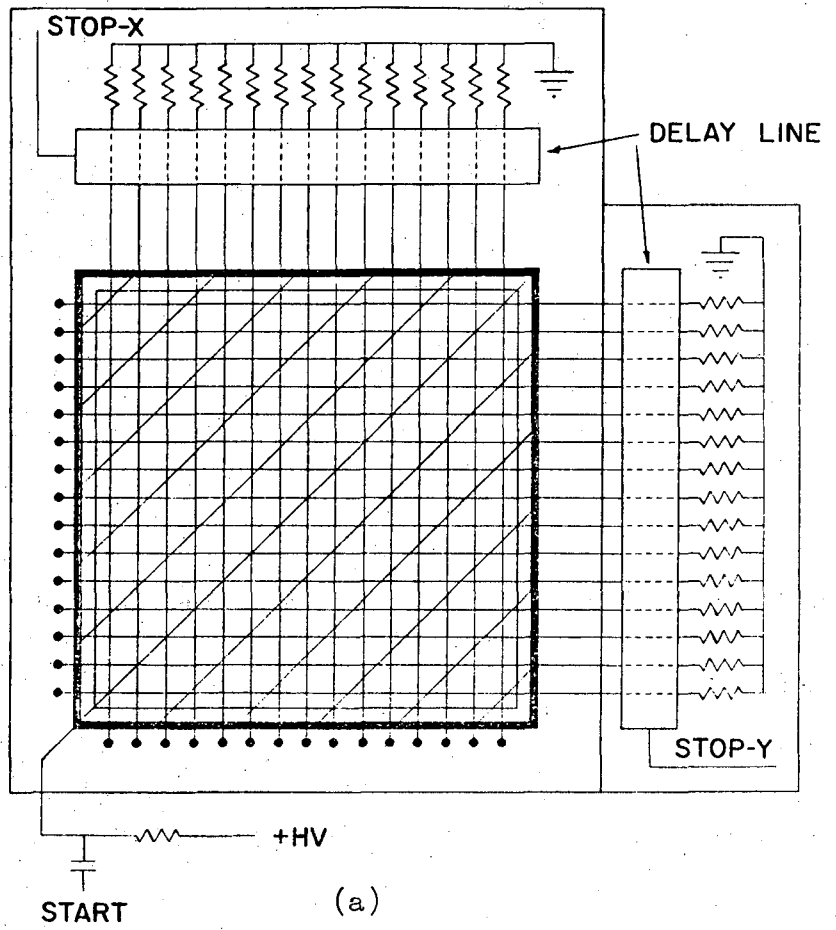
- Fig. 1. Schematic diagram of basic chamber (a) as viewed normally and (b) in a sectional side view. The multiplication wires are oriented at 45° with respect to the ground-plane wires.
- Fig. 2. Electromagnetic delay line showing (a) a 3-view engineering drawing of the assembled line and (b) sketches of typical input-output wave forms.
- Fig. 3. Electronics block diagrams for (a) an analog system with scope display and (b) a digital system with storage capability.
- Fig. 4. Energy spectra obtained with the MWPC. (a) ^{109}Cd , (b) ^{241}Am , (c) fluorescent spectrum from a 10% I solution. The energy resolution is on the order of 17% FWHM.
- Fig. 5. Efficiency and sensitivity (in collected events per cm^2 for each roentgen reaching the detector) for a MWPC of 4 cm thickness, filled with a 90% Xe - 10% CO_2 gas mixture at atmospheric pressure.
- Fig. 6. MTF for 22 keV x-rays. The data points \bullet show the measured contrast ratios for the centerpoints of the test patterns. The dashed curve is the calculated fit to these points, and the solid curve is the corresponding modulation transfer function. (The sign of the 0.5 mm^{-1} datum point is inferred from the fit.)

- Fig. 7. X-ray transmission pictures of philodendron leaves taken with a 0.03 mR exposure at 5.9 keV.
- Fig. 8. X-ray transmission pictures taken with exposures of: (a) 0.015 mR, (b) 0.030 mR, (c) 0.045 mR, and (d) 0.038 mR at 22 keV.
- Fig. 9. Locus plot showing α -particle track endings for 1.5 MeV α particles originating at various depths in the converter.
- Fig. 10. Electronic images of 5/8-in. stencil letters cut in a 20-mil Cd sheet. Images (b), (c), and (d) were all taken with the same oscilloscope-intensity setting. Image (a) was taken at a lower scope intensity. The horizontal lines are images of the anode wires and are characteristic of magnified images from these chambers (ref. 2).
- Fig. 11. Experimental and calculated contrast ratios vs. spatial frequency, modulation transfer functions (MTF). The experimental α -energy discrimination parameters were estimated to be 0.35 MeV (LLD) and 0.65 MeV (ULD). These are the values used in the comparison calculation.
- Fig. 12. (a) 1 mm, (b) 2 mm, and (c) 4 mm bar patterns imaged with 22 keV photons; (d) 2 mm, (e) 4 mm, and (f) 10 mm bar patterns imaged with 60 keV photons. Effect of Lucite absorbers interposed between the MWPC and the bar pattern on the imaging with 60 keV photons are shown for (g) none, (h) 2.54 cm, and (i) 5.08 cm of Lucite.

Fig. 13. Rat labelled with 300 μCi of ^{125}I . MWPC images are shown with (a) 4000 counts, (b) 20 000 counts, and (c) 80 000 counts. Scintillation camera image with 100 000 counts is shown in (d). This picture was taken a day later and shows radioiodine labelling of the thyroid gland. All pictures were obtained with the NC 1 collimator.

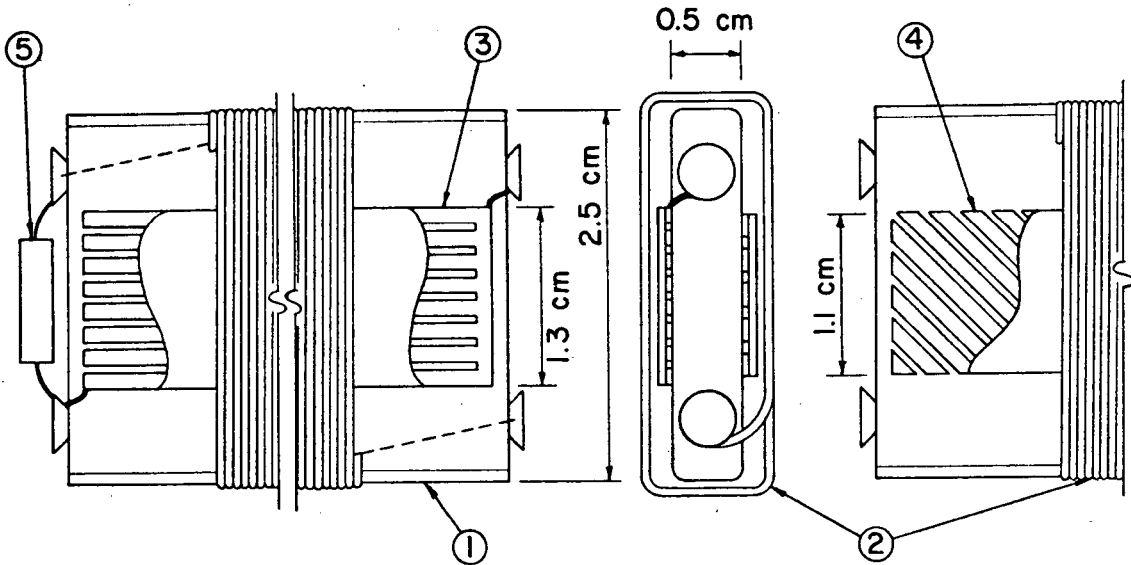
Fig. 14. Schematic diagram comparing laminographic imaging with more conventional radioisotope imaging. In (a) radiation is emitted from the entire organ, whereas in (b) only that plane illuminated by the source emits fluorescence x-rays.

Fig. 15. Schematic of the excitation camera system. The 60 keV γ -rays from the two collimated ^{241}Am line sources excite the characteristic x-rays of natural iodine in the thyroid. The single-channel analyzer permits display only of those photons within the energy band corresponding to the 28.6 keV iodine K_{α} x-ray.

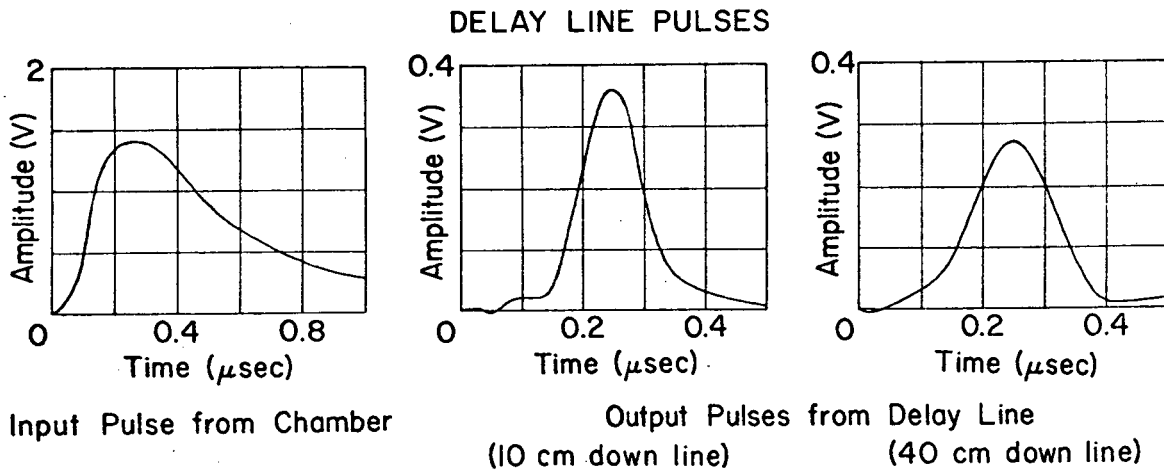


XBL 723-638

Fig. 1

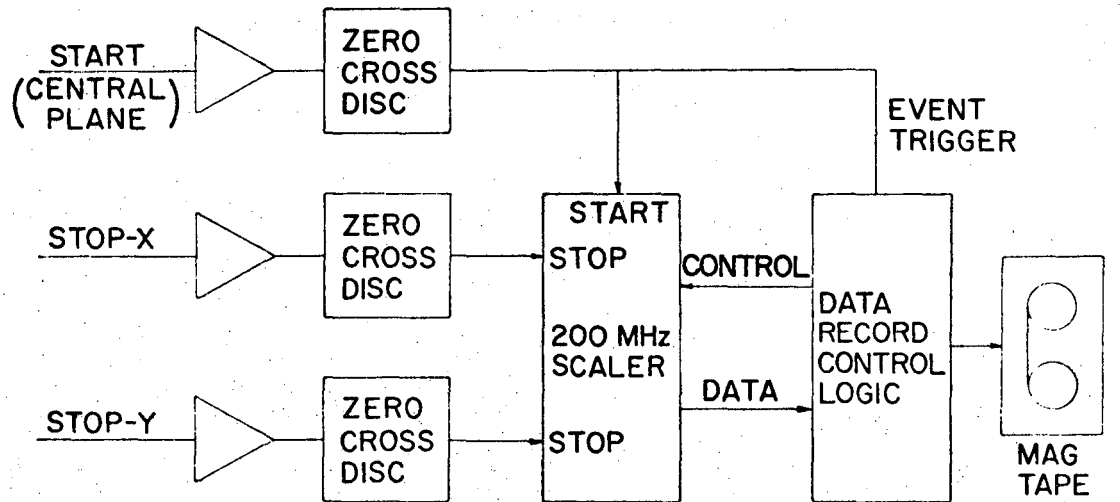
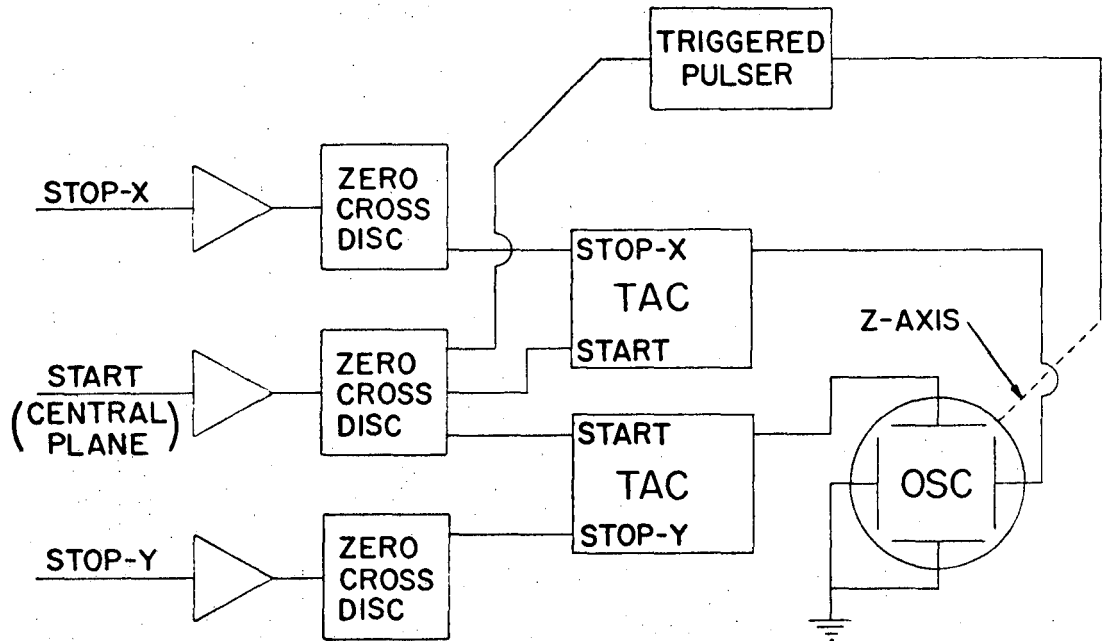


- 1 Plastic Core
- 2 Winding (#38 wire, 8 turns/mm)
- 3 Ground Strips (6.3 strips/cm of 12 μm Al on 25 μm Mylar. Strip width=1.2 mm, gap width=0.4 mm)
- 4 Compensating Strips (Same material as ground strips)
- 5 Terminating Resistor



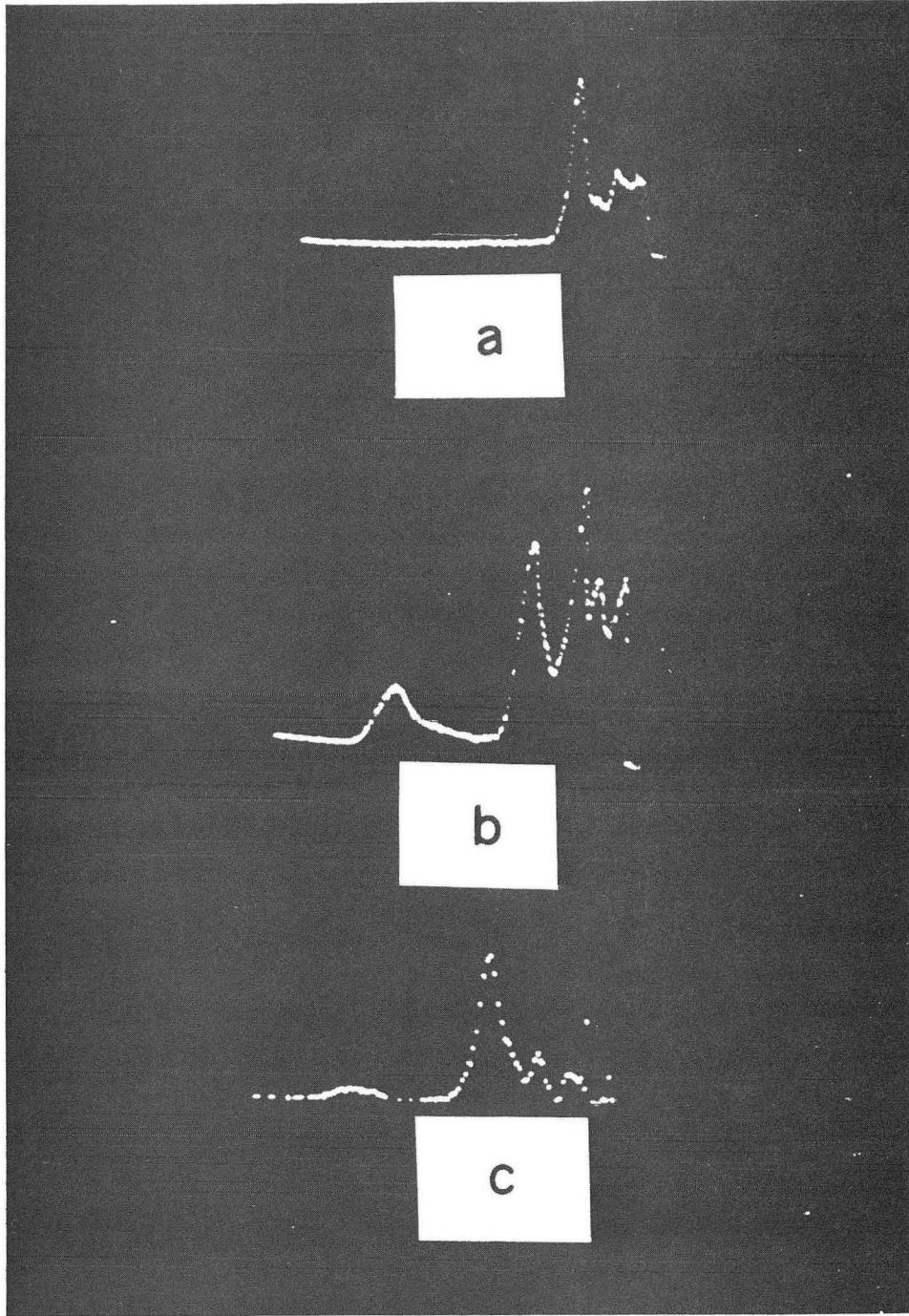
XBL 723-637

Fig. 2



XBL 723-639

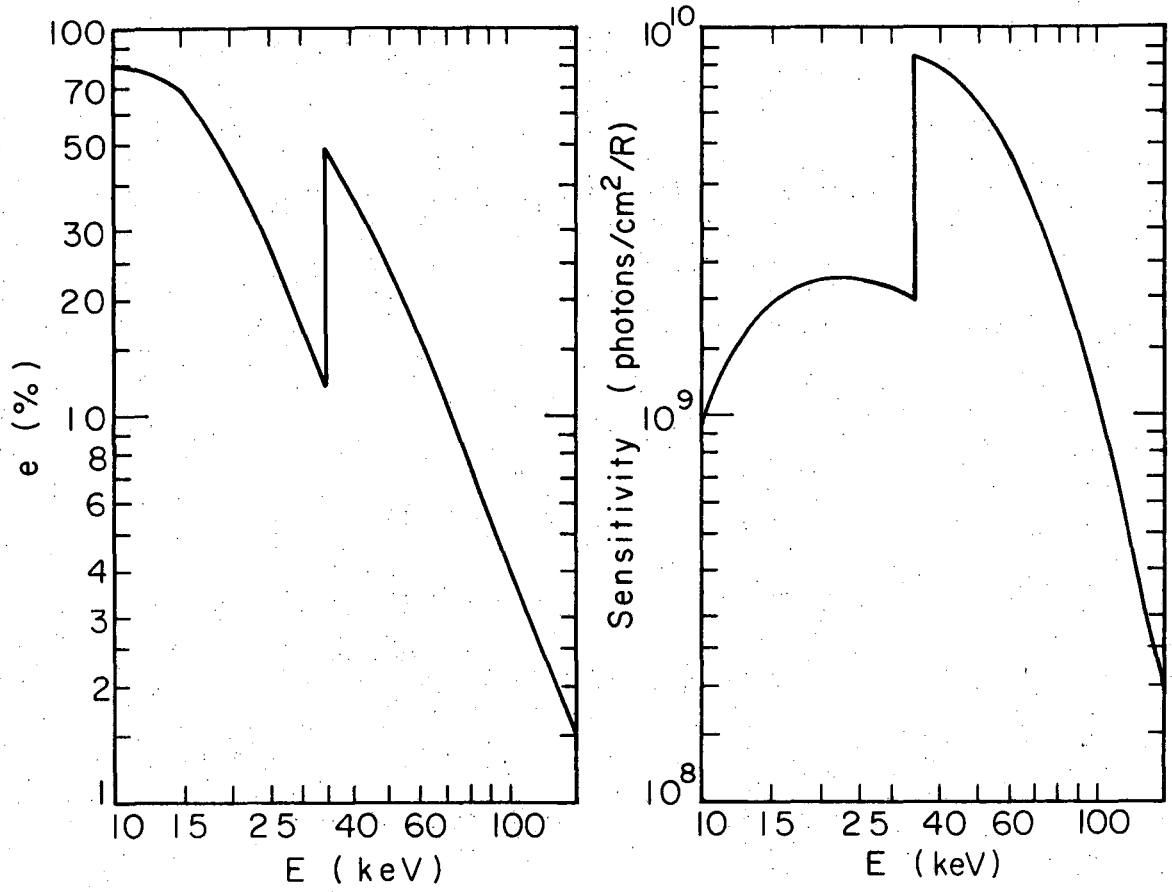
Fig. 3



←
Energy

XBB 725-2905

Fig. 4



XBL722-2316

Fig. 5

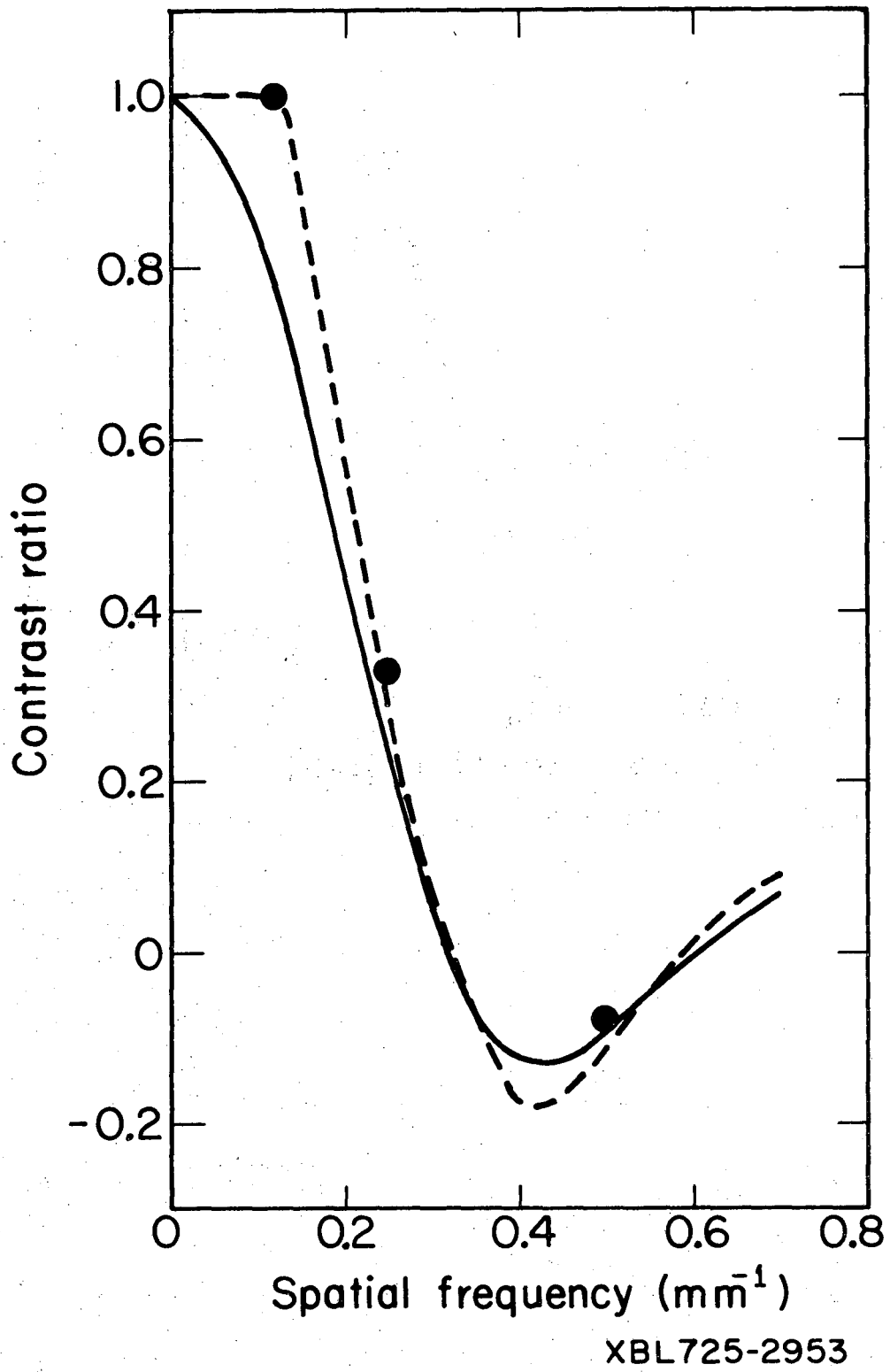
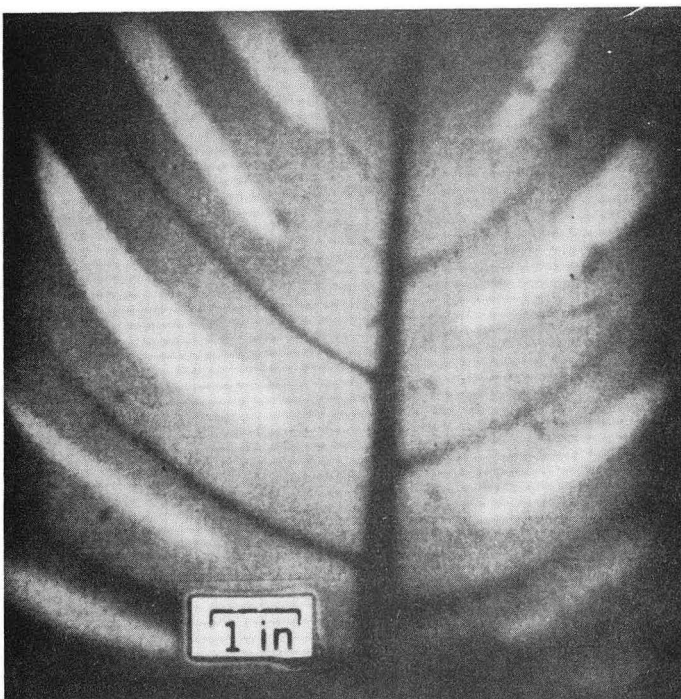
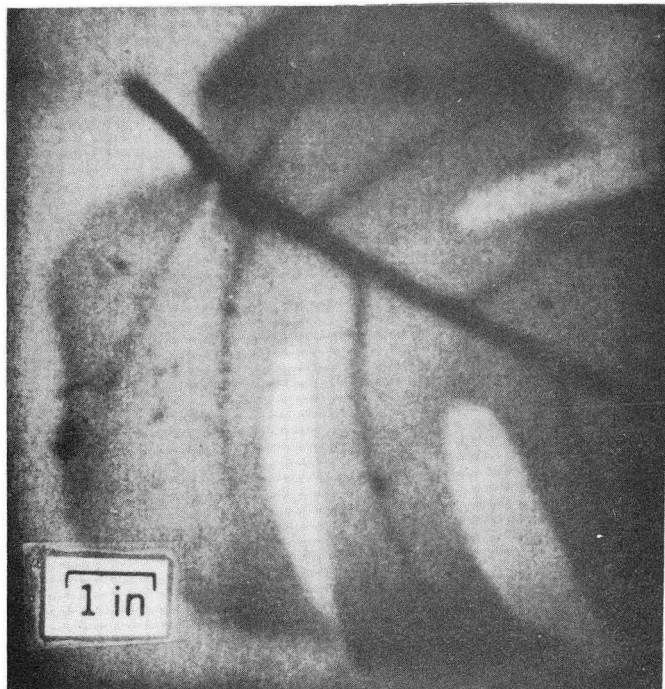
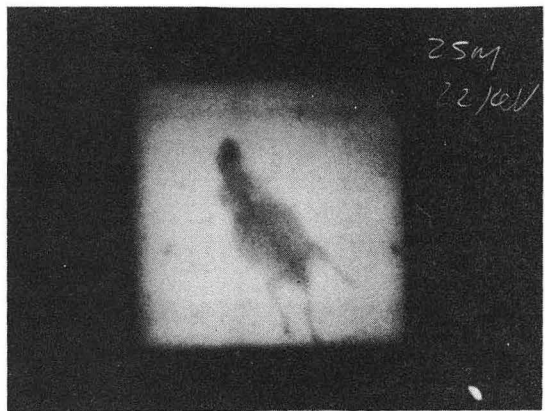
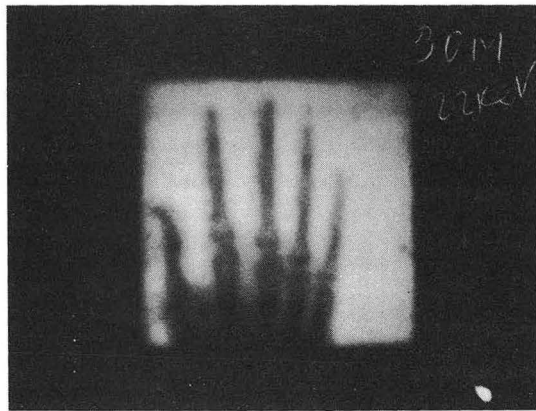
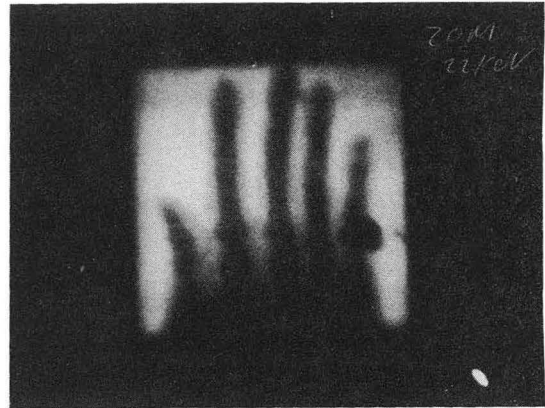
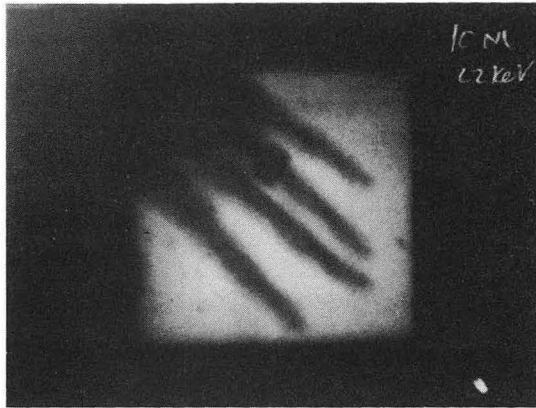


Fig. 6



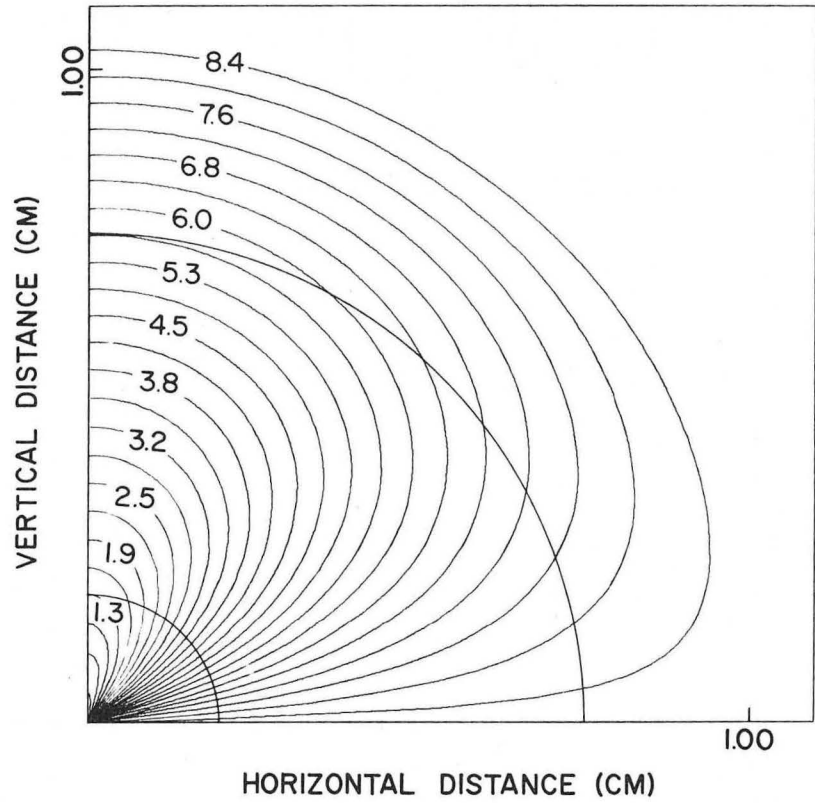
XBB 713-961A

Fig. 7



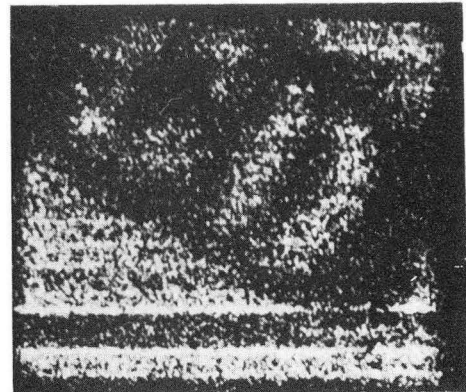
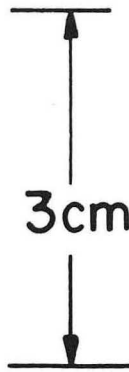
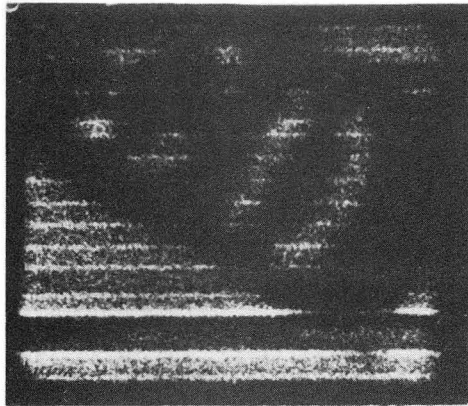
XBB 713-884

Fig. 8



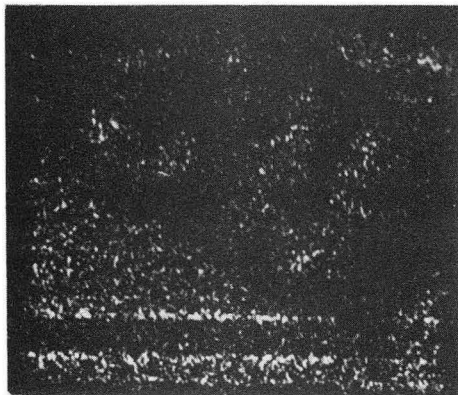
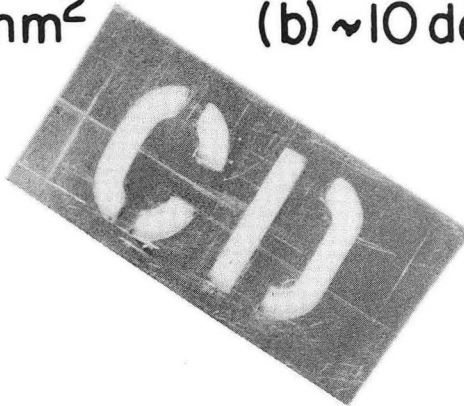
XBL 7110-1590

Fig. 9

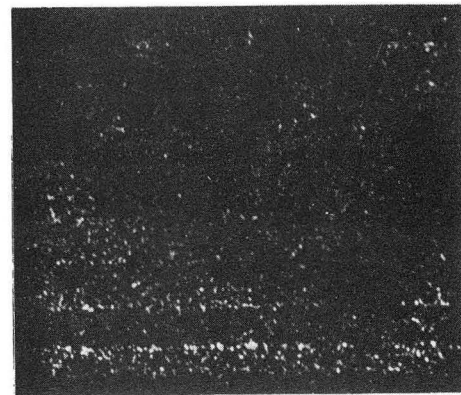


(a) ~ 100 dots/mm²

(b) ~ 10 dots/mm²



(c) ~ 2 dots/mm²



(d) ~ 1 dot / mm²

XBB 721-286

Fig. 10

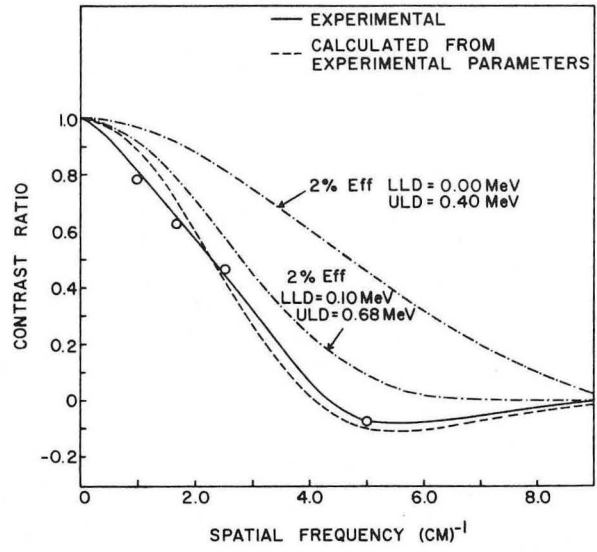
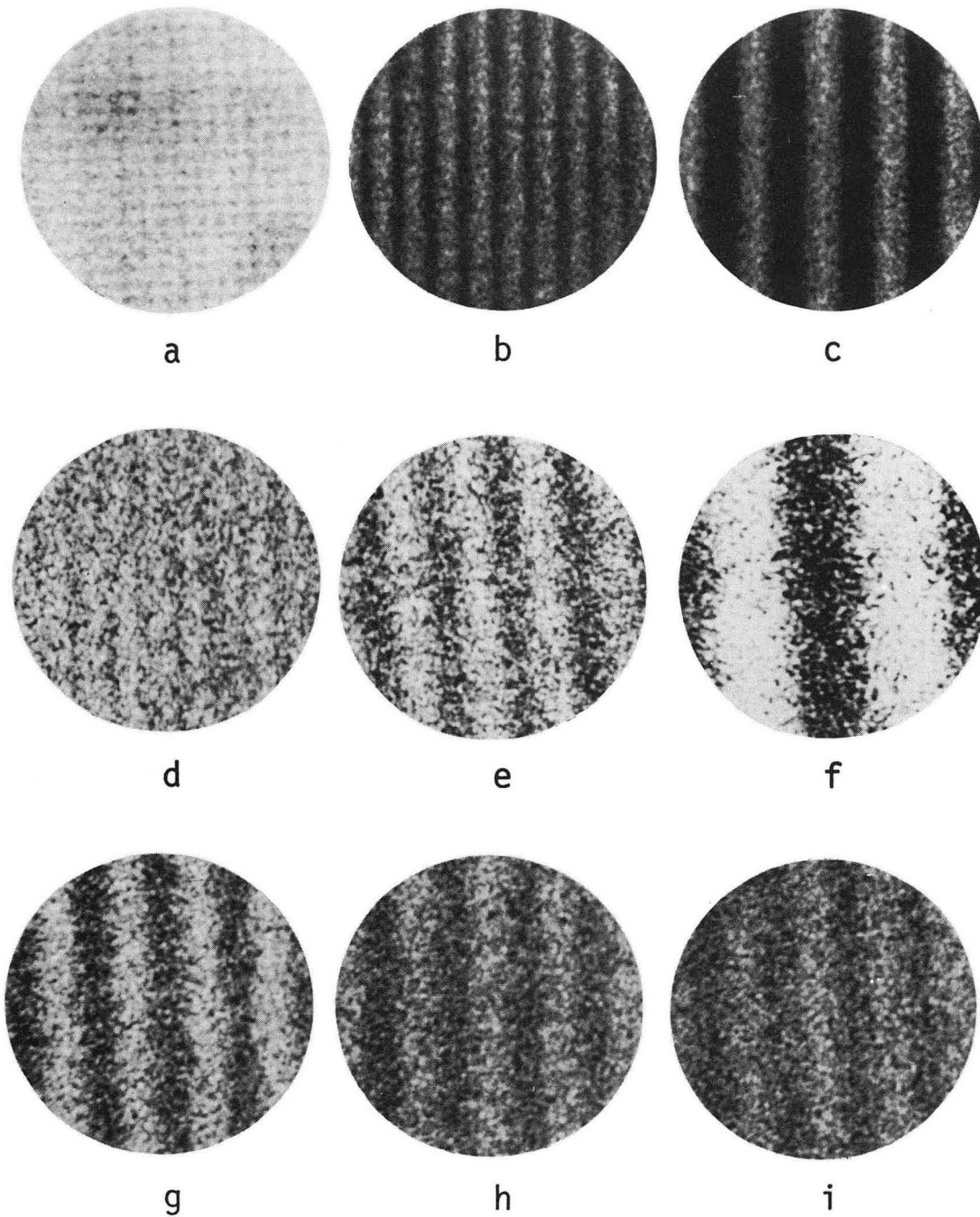
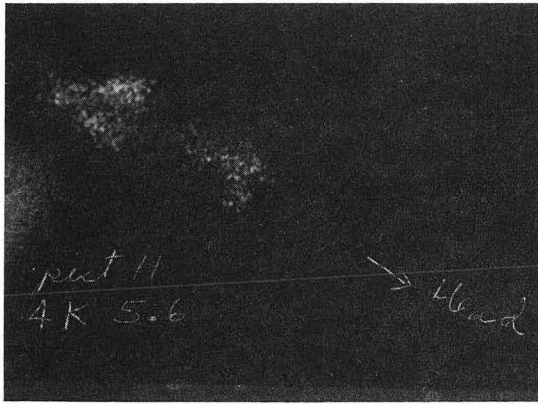


Fig. 11

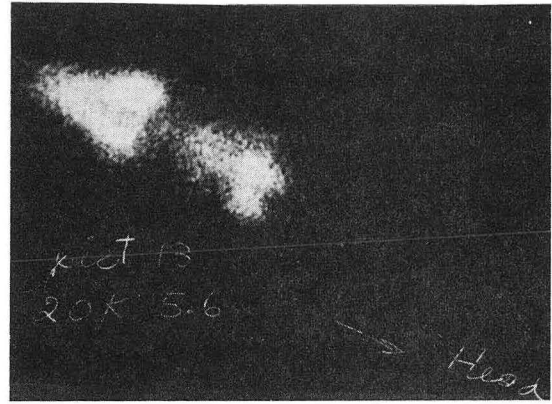


XBB 721-314

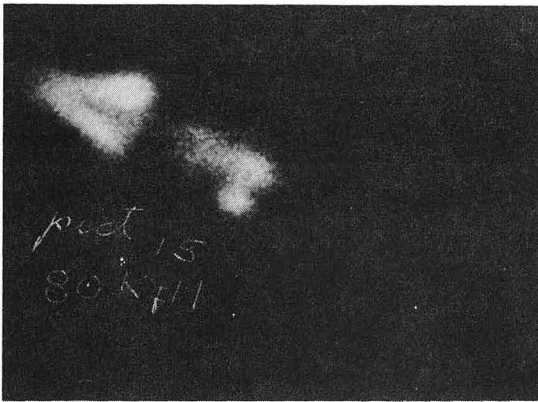
Fig. 12



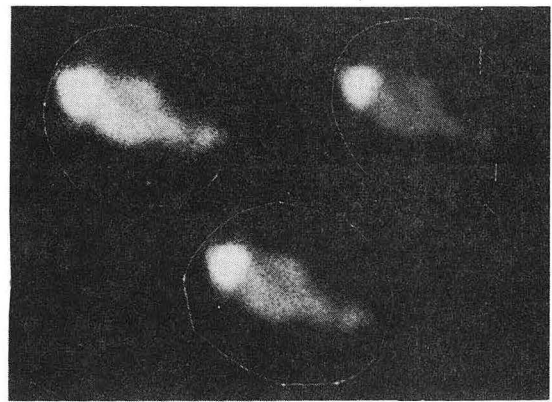
a



b



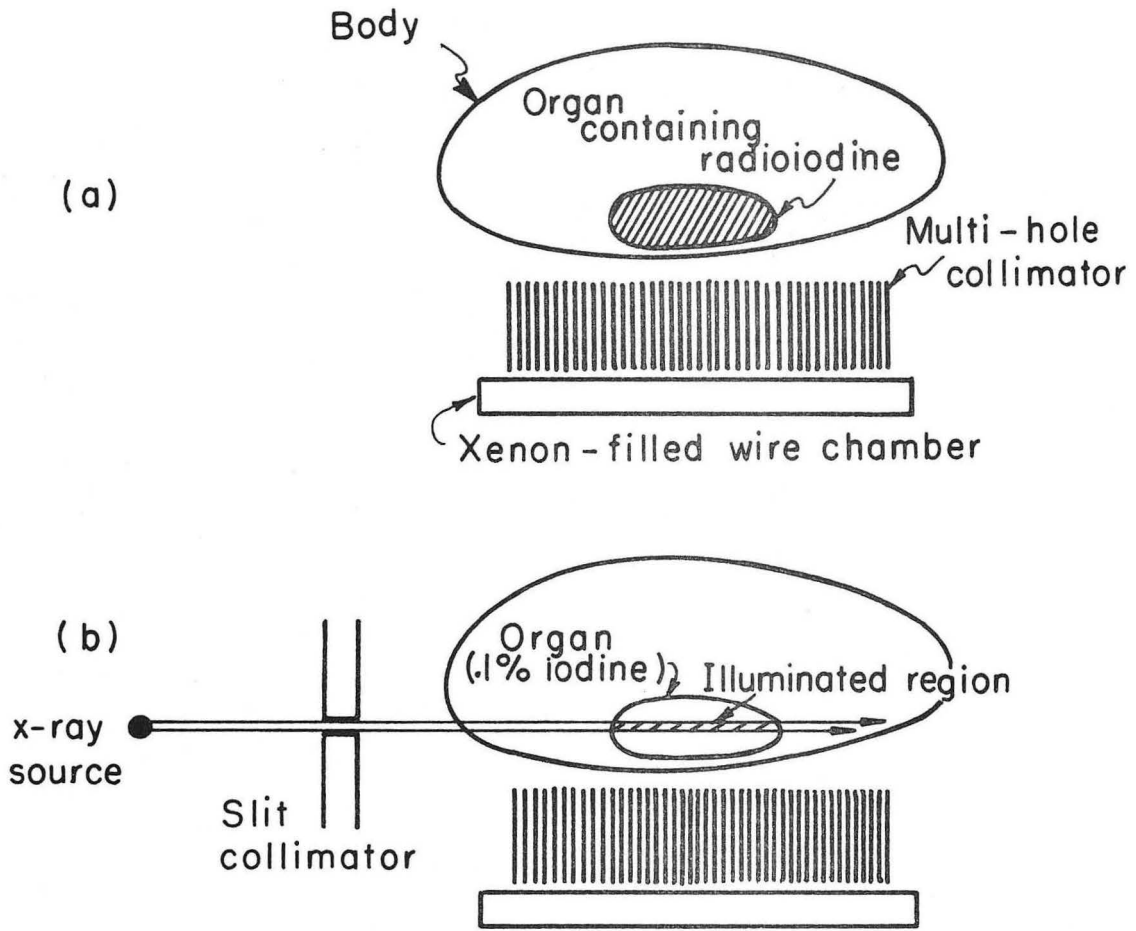
c



d

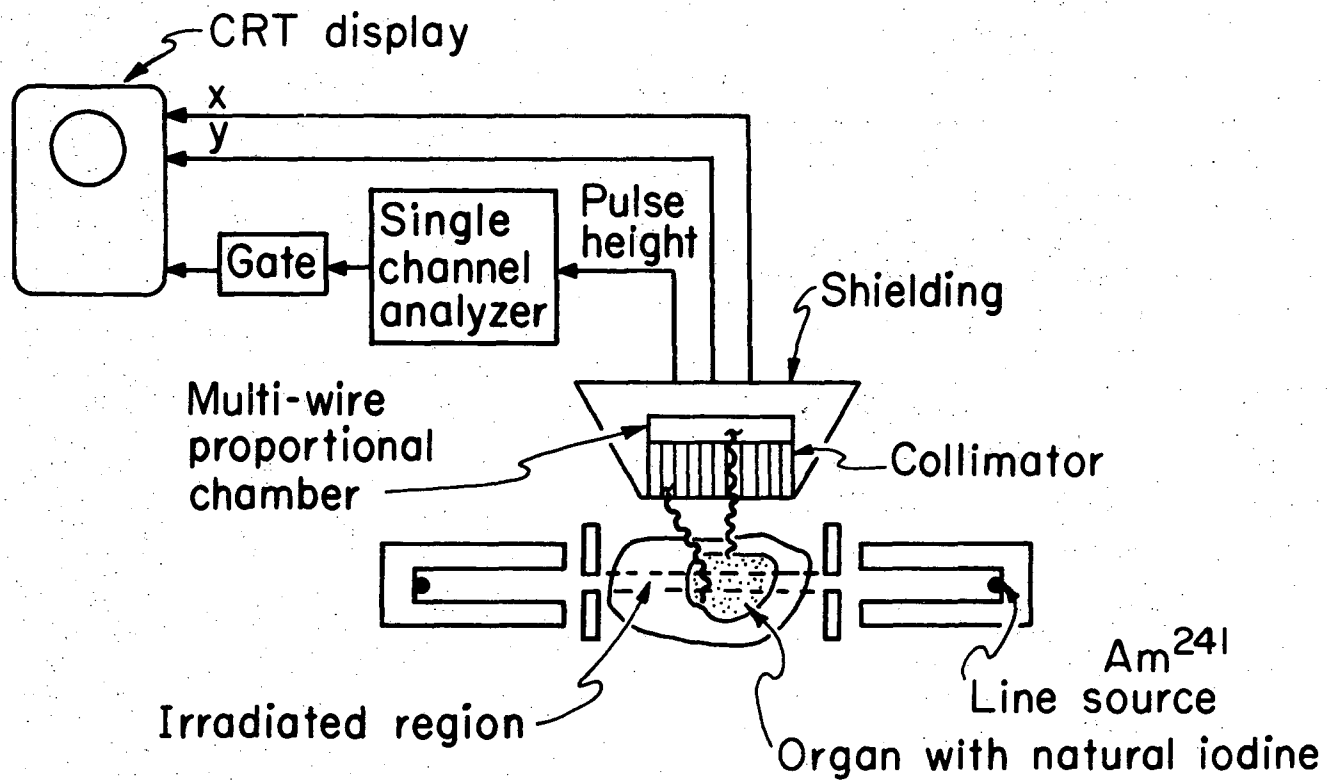
XBB 7110-5089

Fig. 13



XBL 724-2849

Fig. 14



XBL725-2954

Fig. 15

LEGAL NOTICE

This report was prepared as an account of work sponsored by the United States Government. Neither the United States nor the United States Atomic Energy Commission, nor any of their employees, nor any of their contractors, subcontractors, or their employees, makes any warranty, express or implied, or assumes any legal liability or responsibility for the accuracy, completeness or usefulness of any information, apparatus, product or process disclosed, or represents that its use would not infringe privately owned rights.

TECHNICAL INFORMATION DIVISION
LAWRENCE BERKELEY LABORATORY
UNIVERSITY OF CALIFORNIA
BERKELEY, CALIFORNIA 94720